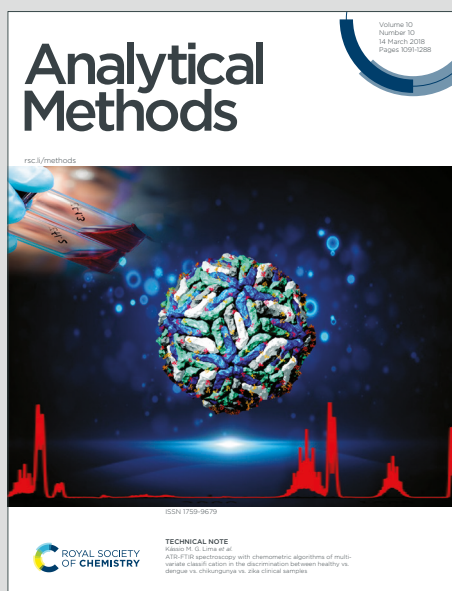


# Analytical Methods

Accepted Manuscript

This article can be cited before page numbers have been issued, to do this please use: L. Gerken, M. W. Rosslein, I. Herrmann and A. Gogos, *Anal. Methods*, 2025, DOI: 10.1039/D5AY00731C.



This is an Accepted Manuscript, which has been through the Royal Society of Chemistry peer review process and has been accepted for publication.

Accepted Manuscripts are published online shortly after acceptance, before technical editing, formatting and proof reading. Using this free service, authors can make their results available to the community, in citable form, before we publish the edited article. We will replace this Accepted Manuscript with the edited and formatted Advance Article as soon as it is available.

You can find more information about Accepted Manuscripts in the [Information for Authors](#).

Please note that technical editing may introduce minor changes to the text and/or graphics, which may alter content. The journal's standard [Terms & Conditions](#) and the [Ethical guidelines](#) still apply. In no event shall the Royal Society of Chemistry be held responsible for any errors or omissions in this Accepted Manuscript or any consequences arising from the use of any information it contains.

# Alternative Digestion Strategy for Ti, Zr and Hf Oxides: Eliminating Hydrofluoric Acid

## Oxides: Eliminating Hydrofluoric Acid

Lukas R. H. Gerken<sup>1,2</sup>, Matthias Roesslein<sup>1</sup>, Inge K. Herrmann<sup>1-4</sup> and Alexander Gogos<sup>1,2\*</sup>

<sup>1</sup>Laboratory for Nanomaterials in Health, Department of Materials Meet Life, Swiss Federal Laboratories for Materials Science and Technology (Empa), Lerchenfeldstrasse 5, 9014 St. Gallen, Switzerland.

<sup>2</sup>Nanoparticle Systems Engineering Laboratory, Institute of Process Engineering, Department of Mechanical and Process Engineering, ETH Zurich, Sonneggstrasse 3, 8092 Zurich, Switzerland.

<sup>3</sup>Ingenuity Lab, University Hospital Balgrist, Forchstrasse 340, 8008 Zurich, Switzerland.

<sup>4</sup>Faculty of Medicine, University of Zurich, Rämistrasse 71, 8006 Zurich, Switzerland.

\* Corresponding author. Tel.: +41 (0)58 765 78 05; e-mail: [alexander.gogos@empa.ch](mailto:alexander.gogos@empa.ch)

**ABSTRACT**View Article Online  
DOI: 10.1039/D5AY00731C

Group IV metal oxides have a broad impact on the environment and human health due to their diverse applications in industry, consumer products and biomedicine. However, their chemical inertness poses significant challenges for accurate quantification in biological matrices, which is essential for assessing biodistribution, toxicity, and regulatory compliance. Traditional digestion methods often rely on hydrofluoric acid (HF), a hazardous reagent requiring specialized handling and infrastructure. Here, we present an alternative, HF-free microwave assisted digestion protocol for group IV metal oxides in biological contexts, utilizing sulfuric acid/water/hydrogen peroxide mixtures to achieve complete solubilization across nano- to microscale particles. The method's efficacy was evaluated on various commercially available TiO<sub>2</sub>, ZrO<sub>2</sub>, and HfO<sub>2</sub> powders. Optimization of digestion parameters, including acid-to-peroxide ratios, temperature, and reaction time, led to recoveries exceeding 90% for all tested materials. Notably, higher temperatures and extended digestion times were required for larger particles and higher atomic number oxides, reflecting the increased metal–oxygen bond dissociation energies. The method's applicability was further demonstrated through successful quantification of spiked nanoparticles in human cancer cells and bovine liver tissue, with detection limits down to ~1ppb and achieving recoveries within 80–100%, maintaining sample stability over four weeks. Comparative analysis with HF-based digestion revealed comparable sensitivity and detection limits using inductively coupled plasma optical emission spectrometry (ICP-OES), with the HF-free method offering a safer and more accessible alternative for routine laboratory analysis. This validated protocol facilitates accurate quantification of group IV metal oxides in complex biological matrices, supporting preclinical and clinical studies while mitigating the risks associated with HF usage.

## 45 INTRODUCTION

46 Group IV metal (Ti, Zr, Hf)-containing materials are utilized in various biomedical and  
47 consumer-good applications, including cancer therapy, dental and orthopaedic implants,  
48 pigments, catalysts and coatings.<sup>1–10</sup> This is primarily due to their biocompatibility and  
49 desirable mechanical, electrical or (physico)chemical properties. For instance, Ti and Ti alloys  
50 (e.g., Ti<sub>6</sub>Al<sub>4</sub>V) are employed in long-lasting, load-bearing medical implants due to their elastic  
51 modulus, which closely resembles that of bone, and their naturally occurring oxide surface.  
52 Zirconium oxide (ZrO<sub>2</sub>) serves as a dental ceramic implant material owing to its white color,  
53 high biocompatibility, low thermal conductivity, toughness, and low bacterial attraction.<sup>11,12</sup>  
54 Although these materials are typically used as bulk implants, it is now well documented (e.g.,  
55 refs<sup>13–15</sup>) that wear particles are released and accumulate in surrounding tissues, highlighting  
56 an increasing need for biodistribution analysis and a better understanding of their material fate.  
57 In nanoparticulate form, group IV metal oxides and metal–organic frameworks (MOFs) show  
58 promise as anticancer agents due to their photocatalytic, radiocatalytic, or high-Z X-ray  
59 absorption properties.<sup>16</sup> For example, nano-TiO<sub>2</sub> exhibits significant photocatalytic activity and  
60 can be used in photodynamic cancer therapies.<sup>17</sup> Similarly, Zr- and Hf-carrying nanomaterials  
61 demonstrate promising X-ray radiation-based anticancer effects.<sup>18–20</sup> Some of these materials  
62 are under clinical investigation,<sup>21,22</sup> or have received regulatory approval for pharmaceutical  
63 applications (e.g., by the FDA).<sup>23</sup> All in all, the various use cases in research suggest group IV  
64 metals will have increasing impact in the future.

65 For clinical translation, it is imperative to gain insights into the stability, biotransformation,  
66 uptake behavior, and biodistribution of these materials. Additionally, metal analysis in tissues  
67 surrounding medical implants is necessary to understand tissue reactions and the release of  
68 metal ions or wear particles.<sup>24</sup> Therefore, there is a growing need to quantify these materials  
69 in different complex matrices such as culture media, blood, cells and tissues. This is also  
70 reflected in demands from regulatory authorities such as the FDA<sup>25</sup>, that emphasize  
71 biodistribution and uptake studies, especially for non-biodegradable materials.

1  
2  
3 72 However, non-validated methods are often used in the bio-medical community (e.g. aqua regia  
4 for Hf<sup>26,27</sup>) or actual concentrations are not even determined<sup>28</sup>. Validated methods for  
5 73 for Hf<sup>26,27</sup>) or actual concentrations are not even determined<sup>28</sup>. Validated methods for  
6 74 determining group IV oxides are often either hazardous or labour-intensive and therefore often  
7 75 not performed or implementable in standard labs. Due to passivation, TiO<sub>2</sub> as well as ZrO<sub>2</sub> and  
8 76 HfO<sub>2</sub> do not dissolve in cold mineral acids with the exception of hydrofluoric acid (HF)<sup>29</sup>.  
9 77 Consequently, most common digestion protocols involve HF in combination with other acids,  
10 78 such as nitric acid (HNO<sub>3</sub>) to break down the oxides and stabilize the analyte ions as fluoride  
11 79 complexes. The use of HF necessitates stringent safety measures and trained personnel as it  
12 80 poses significant health risks upon skin contact and requires immediate medical action upon  
13 81 an incident. Due to these risks and associated costs, alternative digestion methods have been  
14 82 explored, particularly for TiO<sub>2</sub>, one of the most studied nanoscale inorganic materials. Most  
15 83 commonly, fusion reactions have been shown to break down TiO<sub>2</sub>. For example, SiO<sub>2</sub> has  
16 84 been determined in a TiO<sub>2</sub> matrix using alkali fusion with KOH and boric acid, followed by  
17 85 dissolution in dilute HCl<sup>30</sup>. Many other methods rely on fusion with sulfates. For instance, TiO<sub>2</sub>  
18 86 has been determined in sunscreens using a three-step sequential microwave digestion in a  
19 87 1:1 mixture of HNO<sub>3</sub>/HCl followed by fusion in a crucible with KHSO<sub>4</sub> and subsequent  
20 88 dissolution in H<sub>2</sub>SO<sub>4</sub><sup>31</sup>. Furthermore, ammonium persulfate fusion in a crucible followed by  
21 89 soaking in 2% HNO<sub>3</sub> and subsequent hot plate boiling was employed to determine TiO<sub>2</sub> in  
22 90 water and wastewater<sup>32</sup>. Titanium dioxide has also been analyzed in chewing gum by heating  
23 91 a sulfuric acid and catalyst mixture to 400°C for 2 hours in a Kjeldahl unit, followed by dilution  
24 92 to 10% H<sub>2</sub>SO<sub>4</sub> for measurement<sup>33</sup>.  
25 93 The success of such sulfate-based alternative methods is not surprising, since TiO<sub>2</sub> in  
26 94 concentrated H<sub>2</sub>SO<sub>4</sub> is known to form Ti(IV)sulfate (Ti(SO<sub>4</sub>)<sub>2</sub>), which is colorless and  
27 95 dissociates in water. Titanium(IV) also forms different complexes in sulfuric solutions, e.g.  
28 96 [Ti(OH)<sub>2</sub>]<sup>2+</sup>, [Ti(OH)<sub>3</sub>]<sup>+</sup>, [Ti(OH)<sub>2</sub>(HSO<sub>4</sub>)]<sub>aq</sub> and [Ti(OH<sub>3</sub>(HSO<sub>4</sub>))]<sub>aq</sub> (cf ref. <sup>29</sup>, p.1526). Similarly,  
29 97 Zr and Hf form sulfates in sulfuric solutions, including (Zr(SO<sub>4</sub>)<sub>2</sub> · 4H<sub>2</sub>O, Hf(SO<sub>4</sub>)<sub>2</sub> · 4H<sub>2</sub>O,  
30 98 Zr(OH)<sub>2</sub>SO<sub>4</sub> and Hf(OH)<sub>2</sub>SO<sub>4</sub> · H<sub>2</sub>O<sup>34</sup>. Therefore, generating sulfate complexes presents a  
31 99 promising route for solubilizing group IV oxides without using HF. For instance, Ma et al. used

1  
2  
3 100 H<sub>2</sub>SO<sub>4</sub> to extract Zr and Hf with recoveries of 89.1 and 81.2%, respectively, from a  
4  
5 101 zirconosilicate<sup>35</sup>. Furthermore, Watkins et al. demonstrated in 2018 that using H<sub>2</sub>SO<sub>4</sub>/water  
6  
7 102 mixtures and heating to 110°C for 8 hours effectively digested nano-TiO<sub>2</sub> in various matrices  
8  
9 103 including water, fish tissue, periphyton and sediment<sup>36</sup>. Based on these results, we evaluated  
10  
11 104 this approach in a previous study, where we achieved recoveries between 96 and 107% for  
12  
13 105 Ti, Ti/Zr and Hf-containing metal-organic frameworks<sup>37</sup>.

14  
15 106 Encouraged by these results, we further evaluated, developed and validated this HF-free  
16  
17 107 digestion method also for the oxides, which were expected to be more difficult to solubilize. In  
18  
19 108 this study, we investigated and validated the use of a sulfuric acid-hydrogen peroxide-based  
20  
21 109 microwave digestion to quantitatively dissolve group IV oxides in nano- and microparticulate  
22  
23 110 form as a cost effective, quick and readily available alternative to HF and fusion-based  
24  
25 111 methods. We assessed the digestion performance of TiO<sub>2</sub>, ZrO<sub>2</sub> and HfO<sub>2</sub> powders with  
26  
27 112 different, clinically and industrially relevant primary particle sizes from several nm up to  
28  
29 113 microns. After optimizing digestion parameters such as temperature, digestion time and  
30  
31 114 acid/peroxide ratios with the parent powders we finally optimized and demonstrated the  
32  
33 115 applicability of the validated method to quantify these materials in cancer cells and tissues.  
34  
35 116

## 117 **MATERIALS & METHODS**

### 118 **Particles, Chemicals and Reagents**

36  
37 119 For our experiments, we chose commercially available materials where applicable to allow for  
38  
39 120 accessibility for future comparative experiments. Most of the metal oxide powders were  
40  
41 121 available from Sigma Aldrich. The respective product and CAS numbers can be found in Table  
42  
43 122 S1 in the supporting information (SI).

44  
45 123 All reagents were of analytical grade unless stated otherwise. Concentrated HNO<sub>3</sub> (69%),  
46  
47 124 H<sub>2</sub>SO<sub>4</sub> (97%), H<sub>2</sub>O<sub>2</sub> (30%) as well as HF (40%) were obtained from Sigma Aldrich. Ultrapure  
48  
49 125 water (18.2 MΩ) was obtained through an ELGA Chorus purification device. NIST-traceable  
50  
51 126 Certified Reference Materials (CRM) for instrument calibration were obtained from Inorganic  
52  
53 127 Ventures.

## 128 **Digestion procedures**

View Article Online  
DOI: 10.1039/D5AY00731C

129 In total, we evaluated five different digestion procedures and compared them to a combination  
130 of HNO<sub>3</sub>, H<sub>2</sub>O<sub>2</sub> and HF as the "gold standard" method of reference for the selected materials.

131 **Method I:** For digestion method I, 1.5 mL HNO<sub>3</sub> (65%) and 1 mL H<sub>2</sub>O<sub>2</sub> (30%) were added to  
132 the weighted particle powder in a quartz glass tube. The samples were digested in 10 mL  
133 quartz tubes closed by a PTFE cap with pressure-exchange opening in a pressurized  
134 microwave (TurboWAVE, MLS GmbH) at 120 bar pressure and 200 °C for 10 mins, after an  
135 initial ramping phase from room temperature to 200°C of 12 mins.

136 **Method II:** For digestion method II, 1 mL ultrapure H<sub>2</sub>O, 1.5 mL H<sub>2</sub>SO<sub>4</sub> (97%) and 1 mL H<sub>2</sub>O<sub>2</sub>  
137 (30%) were added to the weighted particle powder in the quartz digestion tubes. The samples  
138 were digested in the pressurized microwave at 120 bar pressure and 200 °C for 10 mins, after  
139 an initial ramping phase from room temperature to 200°C of 12 mins.

140 **Method III:** For digestion method III, 1 mL ultrapure H<sub>2</sub>O, 1.5 mL H<sub>2</sub>SO<sub>4</sub> and 1 mL H<sub>2</sub>O<sub>2</sub> were  
141 added to the weighted particle powder in the quartz digestion tubes. The samples were  
142 digested in the pressurized microwave at 120 bar pressure and 250 °C for 30 mins, after an  
143 initial ramping phase from room temperature to 250°C of 12 mins.

144 **Method IV:** For digestion method IV, the particle powders were digested in 1.5 mL H<sub>2</sub>SO<sub>4</sub> and  
145 1 mL H<sub>2</sub>O<sub>2</sub> using the otherwise same procedure as in method III. Since the digestion matrix is  
146 an acid piranha solution requiring special precautions<sup>33</sup>, we first placed all quartz digestion  
147 tubes containing the samples into a cold water bath, then added H<sub>2</sub>SO<sub>4</sub> and finally, slowly,  
148 H<sub>2</sub>O<sub>2</sub>. Both reagents did not immediately mix and react, and a short agitation using a vortex  
149 was necessary. After careful agitation, the samples were immediately placed back into the  
150 cold water bath, as in all cases an exothermic reaction could be observed. The reactions  
151 observed were never violent, i.e. we did not observe heating to >>100°C or very extensive  
152 foaming/effervescence or even deflagration.

153 **HF reference method:** For comparison, the HF-digestion was performed by adding 2 mL  
154 HNO<sub>3</sub>, 1 mL H<sub>2</sub>O<sub>2</sub> and lastly 0.3 mL HF (40%) in a protected HF-facility to pre-weighted particle

1  
2  
3 155 powders. Samples were digested in Teflon tubes at 250°C and 120 bar for 10 min after a  
4 temperature ramping time of 15 min using an ultraCLAVE (MLS GmbH) microwave. Article Online  
DOI: 10.1039/D5AY00731C  
5  
6 156  
7 157 After any digestion method, the samples were transferred to conical 50 mL polypropylene test  
8  
9 158 tubes and filled to the mark with ultrapure water and measured without further dilution (unless  
10  
11 159 stated otherwise) using an inductively-coupled plasma optical emission spectrometer (ICP-  
12  
13 160 OES). All measured concentrations and recovery calculations can be found in the SI, in Tables  
14  
15 161 S3 - S7.  
16

### 163 **Instrumentation**

164 For all measurements, an Agilent 5110 ICP-OES was used. Sample introduction was  
165 performed via an SPS4 autosampler connected to a glass concentric nebulizer followed by a  
166 glass cyclonic double pass spray chamber. Operating parameters of the instrument are  
167 summarized in Table S2 (SI). Calibration curves for all elements of interest were made from  
168 single element standards (CRMs) obtained from Inorganic Ventures (Suisse TP product  
169 numbers: CGTI1 (Ti), CGZR1 (Zr) and CGHF1 (Hf)) and were prepared in an acid solution  
170 matched exactly to the respective samples. Specifically, the calibration solution matrix for the  
171 HF-free digestion solutions consisted of 2.91% v/v H<sub>2</sub>SO<sub>4</sub>, corresponding to 1.5 mL H<sub>2</sub>SO<sub>4</sub>  
172 (97%) per 50 mL total volume, whereas that for the HF digestion solutions contained 2% v/v  
173 HNO<sub>3</sub>. Calibrations were additionally verified by measuring a certified multi-element standard  
174 (CCS-5, Inorganic Ventures). Recoveries for all elements were usually >96% in this case. Data  
175 were initially evaluated using the software ICP-Expert (v7.4.1.10449, Agilent Technologies) to  
176 calculate mass concentrations from intensities before they were exported for further analysis.  
177

### 178 **Method development and spiking experiments**

179 Initial method development was carried out with pure powders. To distribute a defined particle  
180 mass to the digestion tubes, first a 1 mg mL<sup>-1</sup> aqueous dispersion of each powder was  
181 prepared by accurately weighing the powder into a small 2 mL glass vial (VWR). After  
182 weighing, ultrapure water was added so that the final mass concentration reached 1 mg mL<sup>-1</sup>.

1  
2  
3 183 From this dispersion, defined aliquots were then distributed to the digestion tubes after  
4 reaching a homogenous sample dispersion using vortex agitation and ultrasonication and it  
5 184 was proceeded as described above. Similarly, for cell spiking experiments, 10  $\mu\text{L}$  of the  
6 185 homogenous nanoparticle dispersion was added to 100.000 HT1080 cancer cells,  
7 186 corresponding to  $< 0.1$  ng metal mass per cell or  $< 10$  wt%. Cells were previously taken from  
8 187 a routinely cultured cell flask. Cells were cultivated in minimum essential medium Eagle (MEM,  
9 188 Sigma-Aldrich) supplemented with 10% fetal calf serum, 1% L-glutamine, 1% penicillin-  
10 189 streptomycin, 1% nonessential amino acids, and 1 mm sodium pyruvate. To detach cells from  
11 190 a flask, HT1080 cells (ATCC CCL121TM) were trypsinized and counted using a  
12 191 hemocytometer. One million cells per mL solution were recovered and 100.000 cells were  
13 192 added to each quartz digestion tube before nanomaterial dispersions were spiked. Standard  
14 193 culturing practices that were used are described elsewhere.<sup>3</sup>  
15 194 For tissue spiking, the CRM BCR 185R (bovine liver, powder) was weighed in approx. 20 mg  
16 195 aliquots to the quartz tubes and mixed with 200  $\mu\text{L}$  of the homogenous particle dispersion,  
17 196 corresponding to  $< 1$  wt% nanomaterial uptake; Clinically relevant cell or tissue uptake  
18 197 scenarios are considered to be below 10 wt% of metal uptake.<sup>39</sup> For instance, for intratumoral  
19 198 nanoparticle injections of NBTXR3 ( $\text{HfO}_2$ ) a total oxide mass of 1.8 wt% should be injected,  
20 199 corresponding to 1.5 wt% of Hf.<sup>40</sup>  
21 200

## 201 202 **Method validation**

203 The accuracy of the method was determined from best estimates for a true value obtained  
204 from own spiking experiments, as no certified reference materials for group IV oxides in  
205 biological material were available. Specifically, the accuracy was evaluated by relating the  
206 measured metal mass,  $m_{meas.}$ , to an expected metal mass (i.e. best estimate for the true  
207 value),  $m_{exp.}$ , as follows:  
208

$$209 \text{ Recovery (\%)} = \frac{m_{meas.}}{m_{exp.}} = \frac{c_{meas.} \cdot V_s}{(m_{MO} \cdot (1 - SR) \cdot f_M) \cdot (V_s)^{-1}}$$

210

211  $m_{meas.}$  = metal mass in the sample

212  $m_{exp.}$  = expected metal mass

213  $c_{meas.}$  = metal concentration in the sample

214  $V_s$  = sample volume

215  $m_{MO}$  = mass of the metal oxide powder

216  $SR$  = water and organic surface residue mass fraction determined from  
217 thermogravimetric analysis (Table 1)

218  $f_M$  = metal mass fraction of the respective metal oxide with 0.848 (M=Hf), 0.740 (M=Zr)  
219 and 0.599 (M=Ti)

220 Furthermore, we determined the method precision according to the following condition<sup>41</sup>:

$$\Delta x(\%) = \frac{|x_1 - x_2|}{\bar{x}} \cdot 100$$

$$\leq \sqrt{2} \cdot 2 \cdot s_{v,rel} \quad (2)$$

222  $\Delta x(\%)$  = relative difference of measured values to the mean

223  $x_{1,2}$  = measured values

224  $\bar{x}$  = average of measured values

225  $\sqrt{2}$  = root of replicate number (n=2)

226  $s_{v,rel}$  = relative standard deviation - set to a limit of 2%

227 In our case for method II-IV, this condition was fulfilled with  $\overline{\Delta x} = 2.8\% \leq \sqrt{2} \cdot 2 \cdot 2\% = 5.65$ ,  
228 hence digestions were performed in duplicates. All experimentally determined as well as  
229 calculated values for each experiment can be found in Tables S3-7 in the SI. Furthermore,  
230 sample stability was determined by measuring the same samples after a specific time with a  
231 fresh calibration.

232

### 233 Thermogravimetric Analysis

234 Water and Organic surface content was assessed using thermogravimetric analysis (TGA) and  
235 was performed with a NETZSCH TG 209 F1 instrument (NETZSCH-Gerätebau GmbH, Selb,  
236 Germany) and heating of the weighted sample at room temperature to 700 °C, with a heating



237 rate of 10 °C/min under nitrogen flow. The surface residue mass fraction (SR) was quantified  
238 from the weight loss at 700 °C.

239

## 240 X-ray Diffraction

241 X-ray Powder Diffraction was performed on a PANalytical X'Pert Powder Diffractometer  
242 (Malvern Panalytical, UK) equipped with a copper X-ray source. Particle powders were placed  
243 on a low background sample holder and diffraction patterns were recorded from the rotating  
244 powder sample. Rietveld refinement for phase and grain size analysis was performed using  
245 Profex<sup>42</sup> (Version 4.3.5).

246

## 247 RESULTS & DISCUSSION

### 248 Particle characterization and reference digestion

249 Prior to determining element/oxide recoveries, all nano- and microparticles were characterized  
250 to confirm or estimate the theoretical element composition, their sizes and potential organic  
251 surface residues. X-ray powder diffraction (XRD) patterns indicated that all particles were  
252 crystalline (SI, Figure S1). Based on XRD Rietveld refinement calculations, nanoparticles had  
253 grain sizes around 9 – 25 nm, while microparticles ranged from 26 – 107 nm (Table 1). Phase  
254 analysis identified typical metal oxide specific phases. While most particles were present in a  
255 major single phase, nano HfO<sub>2</sub> and nano TiO<sub>2</sub> displayed multiple phases. The analysis also  
256 confirmed the respective phases for micro anatase TiO<sub>2</sub> and micro rutile TiO<sub>2</sub> as specified by  
257 the distributor. Transmission electron microscopy (TEM) corroborated the nanometer-scale  
258 sizes, ranging from 6 to 34 nm ( $d_{\text{TEM}}$ ), suggesting a single crystalline domain per nanoparticle.  
259 Hafnium dioxide was the smallest nanoparticle, followed by TiO<sub>2</sub> and ZrO<sub>2</sub>. The sizes of all  
260 microparticles were estimated using scanning electron microscopy (SEM) images and were  
261 well above the XRD grain sizes, implying multiple crystalline domains per microparticle. HfO<sub>2</sub>,  
262 ZrO<sub>2</sub> and anatase TiO<sub>2</sub> exhibited average particle sizes between 150 and 280 nm ( $d_{\text{SEM}}$ ). Rutile  
263 TiO<sub>2</sub> was the biggest microparticle with an average size of 860 nm. All nano- and microparticles  
264 were spherical to elliptical in shape (SI, Figure S2). Given that nanomaterials possess a higher

1  
2  
3 265 surface area than micromaterials, they are more prone to adsorbing moisture or other volatile  
4 organic substances on their surface. To estimate the amount of such surface adsorbed volatile  
5 266 substances, and with this also the inorganic metal oxide particle weight, thermogravimetric  
6 267 analysis (TGA) was performed (SI, Figure S3). Microparticles exhibited minimal mass loss  
7 268 (<0.2%) after heating to 700 °C, as expected. In contrast, nanoparticles showed notable  
8 269 volatile organic surface residues ranging from 0.7 to 2.6 wt%. Interestingly, the amount of  
9 270 surface residues was highest for the smallest nanoparticle and decreased with particle size,  
10 271 which is in line with the higher surface area of smaller nanoparticles. These surface residues  
11 272 were accounted for in calculating the metal oxide purity correction factor (1-SR, eq.1).  
12 273 Subsequently, metal recovery investigations were performed using ICP-OES with the state-of-  
13 274 the-art HF digestion method as a reference for developing an HF-free digestion method. As  
14 275 expected, the HF method efficiently solubilized the selected materials, yielding recoveries  
15 276 between 93 and 106%. For nano HfO<sub>2</sub>, we noted an increased recovery of slightly over 100%,  
16 277 which might be attributed to minor contaminations. However, all recoveries were compliant to  
17 278 FDA criteria; According to the FDA, an acceptable recovery range for an element in drug  
18 279 testing is between 80% and 120% of the declared content to ensure method accuracy and  
19 280 reliability<sup>43</sup>.  
20 281 Furthermore, we noted impurities of Zr in Hf oxide and vice versa. The metal impurity of Zr in  
21 282 HfO<sub>2</sub> materials was quantified to be < 0.2 % (micro) and < 1.2 % (nano) (Zr/Hf). The impurity  
22 283 of Hf in ZrO<sub>2</sub> materials, however, was around ~ 2 % (Hf/Zr) (SI, Table S3). These impurities  
23 284 were excluded from the recovery calculations. Zirconium (Zr) and Hafnium (Hf) commonly  
24 285 coexist in natural minerals<sup>44</sup> making them mutual impurities in each other's materials. Major Zr  
25 286 sources include Zircon (ZrSiO<sub>4</sub>) and baddeleyite (natural form of ZrO<sub>2</sub>) in which Zr and Hf  
26 287 coexist<sup>45</sup>. Zircon is the primary source of all Hf and contains up to 1.2wt% Hf<sup>45</sup>. Since they are  
27 288 chemically nearly identical, separating these elements remains challenging<sup>45</sup> explaining the  
28 289 observed presence of impurities.  
29 290  
30 291  
31 292

**Table 1:** Material properties (crystal size and phase, particle size and surface residues) of the particles used in this study and calculated oxide recovery rate (eq. 1, SI, Table S3) after HF digestion. Corresponding XRD spectra, EM images and size distributions can be found in the supporting information.

Material	Grain Size		Main Phase	dTEM/SEM Average $\pm$ SD (nm)	Surface Residue, SR Mass Loss (weight %)	Recovery HF reference method (n=2) (%)
HfO <sub>2</sub>	68.1	$\pm 0.4$	Monoclinic (> 99%) <sup>46</sup>	150.4 $\pm$ 66	$\square$ 0.1	95.4 $\pm$ 3.7
ZrO <sub>2</sub>	26.4	$\pm 0.2$	Monoclinic (> 98%) <sup>47</sup>	276.4 $\pm$ 103	$\square$ 0.2	96.4 $\pm$ 1.2
TiO <sub>2</sub>	39.1	$\pm 0.2$	Anatase (> 99%) <sup>48</sup>	218.5 $\pm$ 76	$\square$ 0.1	97.1 $\pm$ 0.4
TiO <sub>2</sub>	127.1	$\pm 1.2$	Rutile (> 96%) <sup>49</sup>	859 $\pm$ 370	$\square$ 0	96.8 $\pm$ 1.2
HfO <sub>2</sub>	8.9	$\pm 1.1$	Monoclinic (> 83%) <sup>46</sup>	5.8 $\pm$ 1.5	$\square$ 2.6	105.5 $\pm$ 2.0
	12.4	$\pm 3.5$	Orthorhombic (> 15%) <sup>50</sup>			
ZrO <sub>2</sub>	25.4	$\pm 0.2$	Monoclinic (> 99%) <sup>47</sup>	31 $\pm$ 7.5	$\square$ 0.7	93.5 $\pm$ 1.0
TiO <sub>2</sub>	14.8	$\pm 0.1$	Anatase (> 93%) <sup>48</sup>	16.5 $\pm$ 6.3	$\square$ 2.0	95.5 $\pm$ 0.4
	18.7	$\pm 0.8$	Rutile (> 6%) <sup>49</sup>			

### Digestion method optimization using pure powders

Initially, materials were digested using a commonly employed HF-free method comprising only HNO<sub>3</sub> and H<sub>2</sub>O<sub>2</sub> (method I, Figure 1) and compared to the reference HF digestion. This approach resulted in unacceptably low recoveries (<30%) for all microparticles. Similarly, nano ZrO<sub>2</sub> exhibited a low recovery (~20%) with this simple nitric acid/peroxide digestion. Consequently, this method also did not fulfill our precision criterion (see eq. 2 and SI Table S4), which is expected for such low recoveries. Interestingly, the recovery for nano TiO<sub>2</sub> and nano HfO<sub>2</sub> was found to be around 80%. Compared to microparticles, nanoparticles have a higher accessible surface area increasing digestion probability. Additionally, sufficiently small and colloidally stable nanoparticles are likely to achieve good atomization efficiency in the ICP plasma without complete digestion. For instance, slurries with particles below ~5  $\mu$ m often achieve good atomization in the plasma and recoveries comparable to digested solutions<sup>51,52</sup>. Such size effects could explain the high recoveries of TiO<sub>2</sub> and HfO<sub>2</sub> nanoparticles, which are smaller than nano ZrO<sub>2</sub> and all microparticles, using the simple nitric acid route. Subsequently, nitric acid was replaced with an aqueous 60% H<sub>2</sub>SO<sub>4</sub> mixture (digestion method II). This change significantly improved nanoparticle recoveries to acceptable levels (90 – 100%). Consequently, also the precision was improved considerably to ~1.6  $\Delta$ x(%).

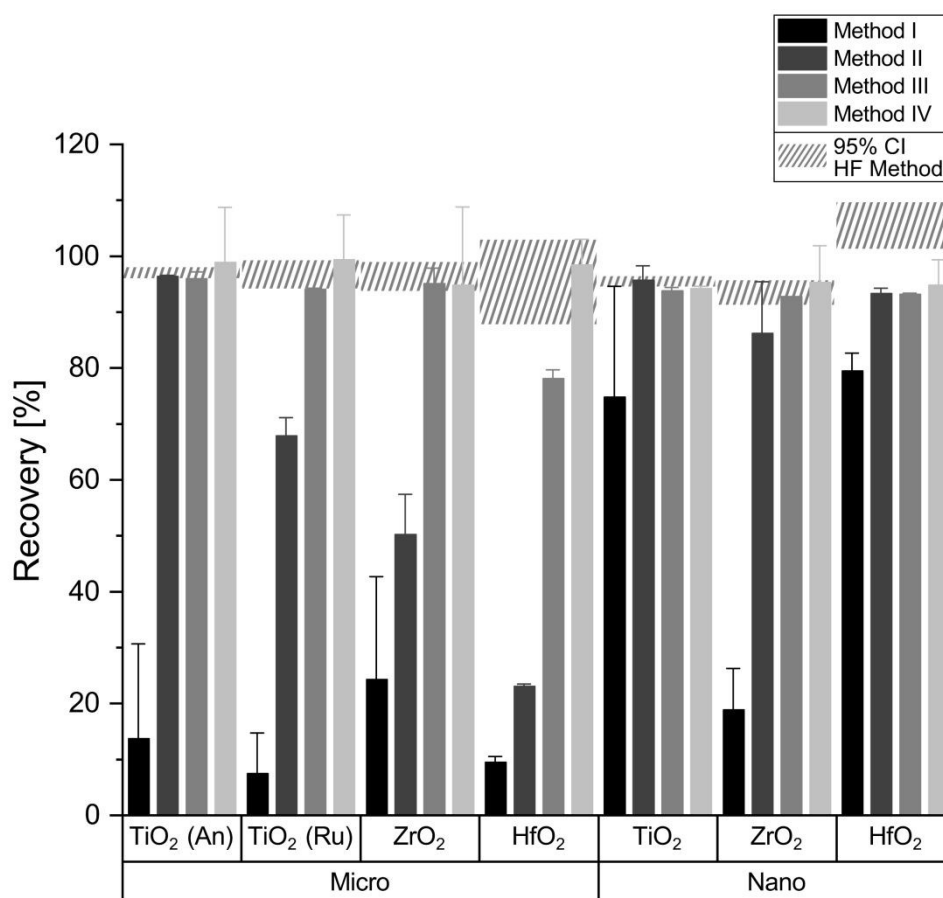
1  
2  
3  
4  
5  
6  
7  
8  
9  
10  
11  
12  
13  
14  
15  
16  
17  
18  
19  
20  
21  
22  
23  
24  
25  
26  
27  
28  
29  
30  
31  
32  
33  
34  
35  
36  
37  
38  
39  
40  
41  
42  
43  
44  
45  
46  
47  
48  
49  
50  
51  
52  
53  
54  
55  
56  
57  
58  
59  
60

Downloaded on 03 June 2025 6:33:28 AM  
This article is licensed under a Creative Commons Attribution 3.0 Unported Licence.



1  
2  
3 316 Microparticle recoveries also improved, following an atomic number (Z) dependent trend.  
4  
5 317 Notably, micro Anatase TiO<sub>2</sub> was recovered at nearly 100% while the Rutile form achieved  
6  
7 318 around 70%. Given that Rutile TiO<sub>2</sub> had a much larger particle size, the differing recoveries  
8  
9 319 between TiO<sub>2</sub> phases likely resulted from size and grain size differences in the micropowders.  
10  
11 320 Compared to TiO<sub>2</sub>, micro ZrO<sub>2</sub> and micro HfO<sub>2</sub> had lower recoveries (~50% and ~20%,  
12  
13 321 respectively). This behavior suggests an atomic number-dependent recovery rate trend,  
14  
15 322 consistent with the Z-dependent increase in metal–oxygen bond dissociation enthalpy for  
16  
17 323 group IV transition metals and oxygen.<sup>53</sup>  
18  
19 324 As microparticle recoveries improved but remained suboptimal, we implemented digestion  
20  
21 325 method III, increasing the target temperature to 250°C and maintaining it for 30 minutes before  
22  
23 326 cooling down. This adjustment tremendously increased microparticle recovery rates;  
24  
25 327 Nanoparticle recovery remained between 90 – 100%, with a slight improvement observed for  
26  
27 328 nano ZrO<sub>2</sub>. Additionally, recovery rates for micro Rutile TiO<sub>2</sub> and micro ZrO<sub>2</sub> exceeded 90%.  
28  
29 329 Only micro HfO<sub>2</sub> showed comparably low recovery rates of just below 80%.  
30  
31 330 To further improve micro HfO<sub>2</sub> digestion, in digestion method IV, we omitted additional water  
32  
33 331 in the digestion matrix, resulting in a more aggressive acid piranha solution (1.5 ml 97% H<sub>2</sub>SO<sub>4</sub>  
34  
35 332 + 1 ml 30% H<sub>2</sub>O<sub>2</sub>) and increased in peroxomonosulfuric acid (Caro's Acid) formation. Handling  
36  
37 333 this solution generally requires special caution<sup>38</sup>. However, in this setting, we never observed  
38  
39 334 excessive heat or gas development, so we consider working to be sufficiently safe. Under  
40  
41 335 these final conditions, all micro- and nanoparticle recovery rates were found to be well above  
42  
43 336 90%.  
44  
45  
46  
47 337  
48  
49  
50  
51  
52  
53  
54  
55  
56  
57  
58  
59  
60

338

View Article Online  
DOI: 10.1039/D5AY00731C

339

340 **Figure 1:** Metal oxide recoveries for micro- and nanopowders and four different digestion methods  
 341 determined from measuring the single elements (Ti, Zr, Hf) and calculated using eq. 1; Method I:  
 342 standard HNO<sub>3</sub>, 10 min @ 200°C, Method II: H<sub>2</sub>SO<sub>4</sub>, 10 min @ 200°C; Method III: H<sub>2</sub>SO<sub>4</sub>, 30 min @  
 343 250°C, Method 4: Piranha, 30 min @ 250°C; An: Anatase, Ru: Rutile. *Error bars signify 2s<sub>rel</sub> (~95%*  
 344 *confidence interval (CI)) and the hatched area the 95% CI of the HF reference method for direct*  
 345 *comparison.*

346

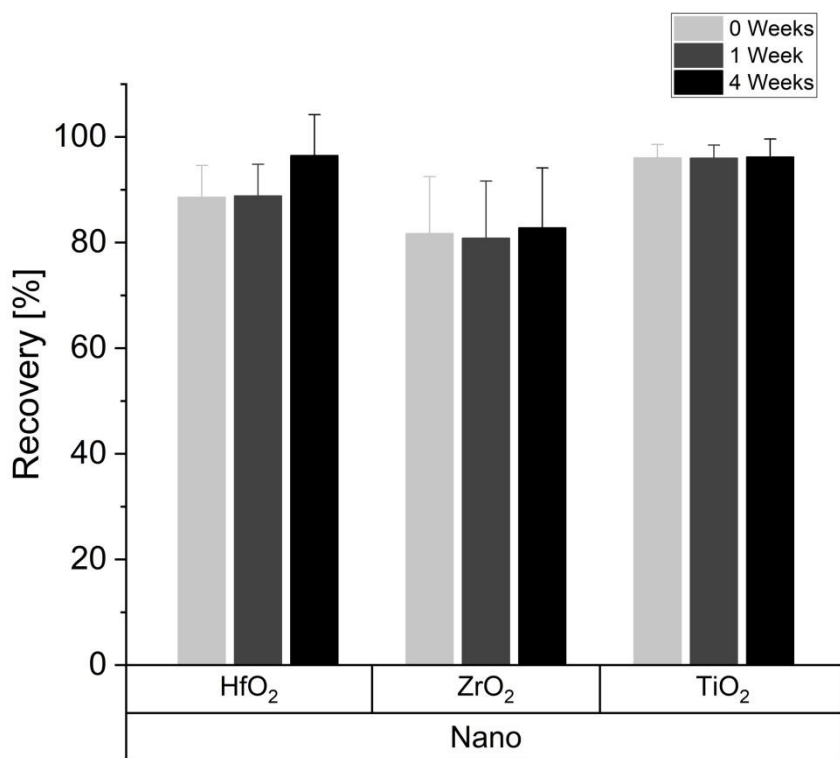
### 347 Application of the optimized method for nanoparticle cell uptake quantification

348 In nanomedical applications, quantifying nanomaterial uptake into cells is crucial for  
 349 understanding nanomaterial-cell interactions. To demonstrate the applicability of the optimized  
 350 HF-free digestion method for cell uptake studies, we used digestion method IV to digest  
 351 nanoparticles spiked to cancer cells (Figure 2) and investigated the stability of the digested  
 352 samples over four weeks. Cells were spiked with nanoparticle concentrations up to 10 wt%,  
 353 representing the higher end of reported cell uptake.<sup>39</sup> All nanoparticles showed recoveries  
 354 between 80% and 100% with a tendency of higher recoveries for TiO<sub>2</sub>, followed by ZrO<sub>2</sub> and



355 HfO<sub>2</sub>. All samples remained stable over the course of 4 weeks, indicating that the metals  
 356 remained stable within the liquid phase, allowing for (re-)evaluation within at least one month.

357



358

359 **Figure 2:** Metal oxide recoveries for nanopowders spiked to cancer cells quantified directly after digestion (0 weeks) using digestion method IV as well as one and four weeks after digestion. Recoveries  
 360 were determined from single element (Ti, Zr, Hf) quantifications and calculations using eq. 1.  
 361 Corresponding nanomaterials were spiked to 100.000 cells per sample resembling a nanomaterial cell-  
 362 uptake scenario between 1 and 10 wt%. Error bars signify  $2s_{rel}$  (~95% confidence interval).  
 363  
 364

### 365 Application and further method optimization in spiked bovine liver tissue

366 For *in vivo* toxicity or efficacy studies, metal recovery in organs or target tissues from  
 367 inserted or injected engineered nano- and micron-sized materials is essential. To  
 368 simulate such scenarios, the optimized digestion method (IV) was applied to bovine  
 369 liver tissue (BCR185r) samples spiked with nano- and micro-metal oxide powders.

370 Metal recoveries were excellent for micro- and nano-TiO<sub>2</sub> as well as for all  
 371 nanopowders (> 90%, Figure 3a). However, the material-dependent decrease in  
 372 recovery observed during the initial method optimization reappeared (e.g., micro: TiO<sub>2</sub>  
 373 (~100%) > ZrO<sub>2</sub> (~85%) > HfO<sub>2</sub> (~70%) / nano: TiO<sub>2</sub> (~100%) = ZrO<sub>2</sub> (~100%) > HfO<sub>2</sub>

1  
2  
3  
4  
5  
6  
7  
8  
9  
10  
11  
12  
13  
14  
15  
16  
17  
18  
19  
20  
21  
22  
23  
24  
25  
26  
27  
28  
29  
30  
31  
32  
33  
34  
35  
36  
37  
38  
39  
40  
41  
42  
43  
44  
45  
46  
47  
48  
49  
50  
51  
52  
53  
54  
55  
56  
57  
58  
59  
60

Downloaded from https://pubs.rsc.org on 03 June 2025 06:33:28 AM  
 This article is licensed under a Creative Commons Attribution 3.0 Unported Licence.



374 (~90%). Extending the reaction time from 30 to 60 minutes increased metal recoveries  
 375 to > 90% for ZrO<sub>2</sub> and HfO<sub>2</sub> micropowders as well as HfO<sub>2</sub> nanoparticles in liver tissue.  
 376 Thus, more complex sample matrices require longer reaction times. Furthermore,  
 377 these results suggest that the method might be also applicable to other types of  
 378 aqueous and/or organic matter containing samples, such as for example wastewater  
 379 or sewage sludge. Overall, HF-free digestion method IV provided excellent group IV  
 380 metal recoveries also in *in vivo* scenarios for both nano- and microparticles.  
 381 Additionally, digested samples displayed a very good long term sample stability post  
 382 digestion of at least four weeks (Figure 3b).

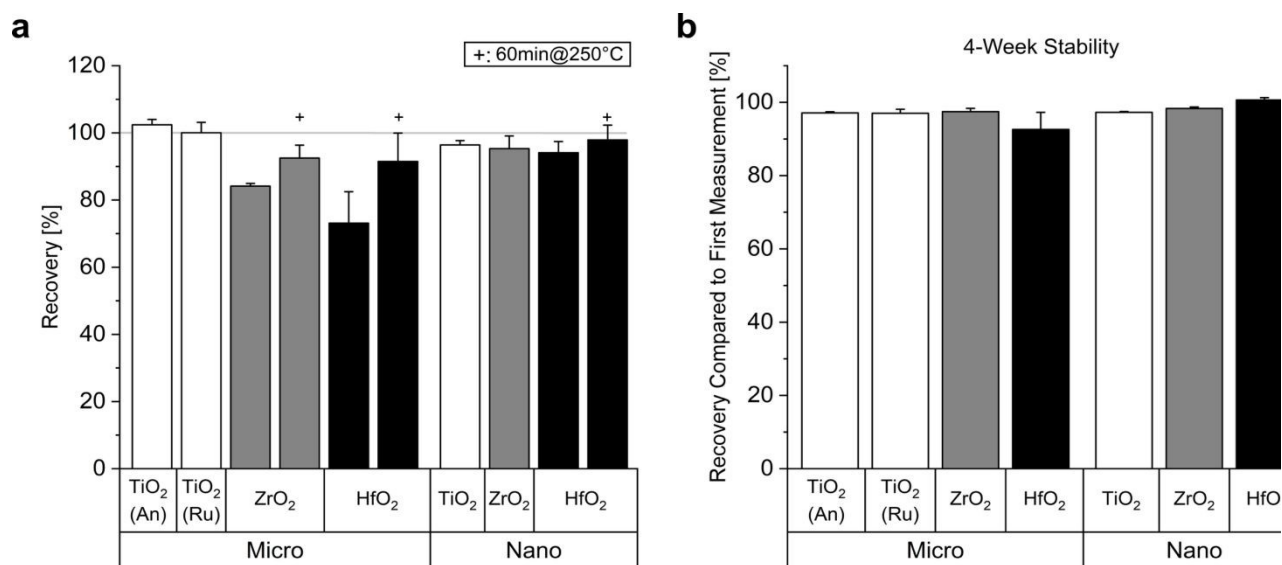


**Figure 3:** (a): Metal oxide recoveries for micro- and nanopowders mixed with bovine liver tissue simulating an *in vivo* scenario after digestion using method IV or an adapted method IV with a longer microwave reaction time at 250°C (60 instead of 30 minutes, indicated by the “+” sign). Recoveries were determined from single element (Ti, Zr, Hf) quantifications and calculations using eq. 1. (b): Four-weeks stability of digested samples plotted as recovery compared to the first measurement in (a) performed directly after digestion; An: Anatase, Ru: Rutile. Error bars signify  $2s_{rel}$  (~95% confidence interval).

### Sensitivity and Detection Limits of HF-free vs. HF digestion method

Finally, ICP-OES detection limits and sensitivity were compared between the HF-free and HF reference digestion method. The detection and quantification limits (*DL* and

*QL*, respectively) were calculated per FDA guidelines:  $DL = \frac{3.3\sigma}{slope}$  and  $QL = \frac{10\sigma}{slope}$ , where

$\sigma$  is the standard deviation of the blank response (here: emission intensity).<sup>43</sup>

1  
2  
3 396 Sensitivities, indicated by calibration slopes (intensity/ppb), were comparable for both  
4  
5 397 methods, following atomic number order (Ti:  $\sim 96$  Int. ppb $^{-1}$  > Zr:  $\sim 88$  Int. ppb $^{-1}$  > Hf:  
6  
7 398  $\sim 5$  Int ppb $^{-1}$ , Table 2). Consequently, detection and quantification limits followed this  
8  
9  
10 399 trend but were generally slightly lower for the HF method. While the instrument and  
11  
12 400 method *DLs* and *QLs* of the HF method were very similar to each other, they showed  
13  
14 401 a discrepancy to those of the HF-free method. This is because the standard deviation  
15  
16 402 of the procedure blanks was generally higher for the HF-free method compared to the  
17  
18 403 HF method. This behavior might be attributed to matrix differences (2.9% H<sub>2</sub>SO<sub>4</sub>  
19  
20 404 compared to 2% HNO<sub>3</sub>) which can affect viscosity and, consequently, nebulization and  
21  
22 405 transport efficacies in both methods. This is supported by the observation that the *DL*  
23  
24 406 and *QL* can be lowered by roughly a factor 2-3 by doubling the readout time (SI, Table  
25  
26 407 S8). Further improvements in *DLs* and *QLs* can be achieved by implementing tube  
27  
28 408 pre-cleaning procedures to prevent analyte carryover between measurement  
29  
30 409 campaigns and by increasing rinsing time between individual measurements.  
31  
32 410 Nevertheless, given the comparable quantification sensitivities and the similar ranges  
33  
34 411 of detection and quantification limits, we conclude that the HF-free method is a viable  
35  
36 412 alternative to the reference HF digestion method which can be used in every standardly  
37  
38 413 equipped analytical laboratory.  
39  
40  
41  
42  
43  
44 414  
45  
46 415  
47  
48 416  
49  
50 417  
51  
52 418  
53  
54 419  
55  
56  
57  
58  
59  
60

**Table 2:** Detection Limit (DL), Quantification Limit (QL) and calibration slope (sensitivity) for each element (Ti, Zr, Hf) for the HF-free and the HF reference digestion method as quantified using ICP-OES.

Limits of Detection	HF-free Method		HF Method		
	Method	Instrument	Method	Instrument	
	[ppb]	[ppb]	[ppb]	[ppb]	
Ti	DL	0.69	0.21	0.37	0.34
	LOQ	2.10	0.63	1.12	1.03
	Slope	96.16 Int. ppb <sup>-1</sup>		96.03 Int. ppb <sup>-1</sup>	
Zr	DL	2.23	0.71	0.86	1.03
	LOQ	6.76	2.14	2.62	3.13
	Slope	88.08 Int. ppb <sup>-1</sup>		89.05 Int. ppb <sup>-1</sup>	
Hf	DL	10.52	1.90	1.95	1.69
	QL	31.87	5.76	5.89	5.13
	Slope	5.27 Int. ppb <sup>-1</sup>		5.35 Int. ppb <sup>-1</sup>	

## CONCLUSION

The reliable detection of group IV metal oxides is playing an increasingly important role in the biomedical as well as environmental fields. To digest group IV metal oxide materials, HF- or fusion-based methods are standardly used to date. Here, we have shown that sulfuric acid and hydrogen peroxide can be used as easily available, comparatively safe alternative HF-free digestion method for Ti, Zr and Hf metal oxides, both as pure powders and in aqueous environments with organic matter (cells, tissues). While nanomaterials were easier to digest, micron-sized powders required higher reaction temperatures, longer reaction times, and higher concentrations of peroxomonosulfuric acid for successful digestion. Digestion efficacy was also atomic number dependent. The proposed methods can be used to quantify the oxide elements in cells, organs and tissues from average particle sizes <6 nm up to 860 nm. ICP-OES revealed good linearity between 0.01 and 5 mg L<sup>-1</sup> (corresponding to 0.005 – 2.5 ng cell<sup>-1</sup>, considering 100 000 digested cells per sample, or, 0.25 – 12.5 mg g<sup>-1</sup> of dried tissue,

Downloaded from https://pubs.rsc.org on 03 June 2025 at 06:33:28 AM. This article is licensed under a Creative Commons Attribution 3.0 Unported Licence.



1  
2  
3 438 considering 20 mg digested tissue per sample) and common metal-dependent detection limits,  
4  
5 439 comparable to those of an HF-containing reference method. The proposed HF-free method  
6  
7 440 has fewer safety and infrastructural demands compared to HF digestions and allows cheaper  
8  
9 441 and easier access to pre-clinical and clinical toxicity as well as efficacy studies with group IV  
10  
11 442 metal oxide materials.  
12  
13  
14 443

#### 15 444 **AUTHOR CONTRIBUTIONS**

16  
17 445 **LRHG:** Investigation, Methodology, Validation, Formal analysis, Data Curation, Writing  
18  
19 446 - Original Draft, Writing - Review & Editing; **MR:** Formal analysis, Writing - Review &  
20  
21 447 Editing; **IKH:** Resources, Funding acquisition, Writing - Review & Editing; **AG:**  
22  
23 448 Conceptualization, Supervision, Validation, Writing - Original Draft, Writing - Review &  
24  
25 449 Editing  
26  
27 450

#### 28 451 **ACKNOWLEDGEMENTS**

29 452 This work received funding from EU Project Metrino (Project number 22HLT04) and  
30  
31 453 the Ria & Arthur Dietschweiler foundation. Andreas Voegelin and Ralf Kaegi (EAWAG)  
32  
33 454 are kindly acknowledged for granting us access to their HF lab as well as Brian Sinnet  
34  
35 455 and Matthias Philipp for on-site support.  
36  
37 456

#### 38 457 **Data availability**

39 458 The data supporting this article have been included as part of the Supplementary  
40  
41 459 Information.  
42  
43 460

#### 44 461 **References**

45 462 (1) Tu, H.-L.; Zhao, H.-B.; Fan, Y.-Y.; Zhang, Q.-Z. Recent Developments in Nonferrous  
46 463 Metals and Related Materials for Biomedical Applications in China: A Review. *Rare Met.*  
47 464 **2022**, *41* (5), 1410–1433. <https://doi.org/10.1007/s12598-021-01905-y>.

- 1  
2  
3 465 (2) Gerken, L. R. H.; Neuer, A. L.; Gschwend, P. M.; Keevend, K.; Gogos, A.; Anthis, A.  
4 466 H. C.; Aengenheister, L.; Pratsinis, S. E.; Plasswilm, L.; Herrmann, I. K. Scalable Synthesis of  
5 467 Ultrasmall Metal Oxide Radio-Enhancers Outperforming Gold. *Chem. Mater.* **2021**, *33* (9),  
6 468 3098–3112. <https://doi.org/10.1021/acs.chemmater.0c04565>.  
7  
8 469 (3) Gerken, L. R. H.; Gogos, A.; Starsich, F. H. L.; David, H.; Gerdes, M. E.; Schiefer, H.;  
9 470 Psoroulas, S.; Meer, D.; Plasswilm, L.; Weber, D. C.; Herrmann, I. K. Catalytic Activity  
10 471 Imperative for Nanoparticle Dose Enhancement in Photon and Proton Therapy. *Nat. Commun.*  
11 472 **2022**, *13* (1), 3248. <https://doi.org/10.1038/s41467-022-30982-5>.  
12  
13 473 (4) Wang, J.; Pan, J.; Tang, Y.; Chen, J.; Fei, X.; Xue, W.; Liu, X. Advances of Hafnium  
14 474 Based Nanomaterials for Cancer Theranostics. *Front. Chem.* **2023**, *11*.  
15 475 <https://doi.org/10.3389/fchem.2023.1283924>.  
16 476 (5) Rehman, F. U.; Zhao, C.; Jiang, H.; Wang, X. Biomedical Applications of Nano-Titania  
17 477 in Theranostics and Photodynamic Therapy. *Biomater. Sci.* **2015**, *4* (1), 40–54.  
18 478 <https://doi.org/10.1039/C5BM00332F>.  
19 479 (6) Bannunah, A. M. Biomedical Applications of Zirconia-Based Nanomaterials:  
20 480 Challenges and Future Perspectives. *Molecules* **2023**, *28* (14), 5428.  
21 481 <https://doi.org/10.3390/molecules28145428>.  
22 482 (7) Wang, J.; Wang, Z.; Wang, W.; Wang, Y.; Hu, X.; Liu, J.; Gong, X.; Miao, W.; Ding,  
23 483 L.; Li, X.; Tang, J. Synthesis, Modification and Application of Titanium Dioxide  
24 484 Nanoparticles: A Review. *Nanoscale* **2022**, *14* (18), 6709–6734.  
25 485 <https://doi.org/10.1039/D1NR08349J>.  
26 486 (8) Chitoria, A. K.; Mir, A.; Shah, M. A. A Review of ZrO<sub>2</sub> Nanoparticles Applications  
27 487 and Recent Advancements. *Ceram. Int.* **2023**, *49* (20), 32343–32358.  
28 488 <https://doi.org/10.1016/j.ceramint.2023.06.296>.  
29 489 (9) Kumar, M.; Halder, S.; Kumar, A. A Review of Biomedical Applications of Zirconia-  
30 490 Based Nanomaterials. In *Advances in Materials Engineering*; Bhingole, P., Joshi, K., Yadav,  
31 491 S. D., Sharma, A., Eds.; Springer Nature: Singapore, 2025; pp 71–81.  
32 492 [https://doi.org/10.1007/978-981-97-7114-1\\_7](https://doi.org/10.1007/978-981-97-7114-1_7).  
33 493 (10) Ayyaru, S.; Jayaraman, V.; Ahn, Y.-H. Non-Precious HfO<sub>2</sub> Nanoparticle as an  
34 494 Alternative Cathode Catalyst for Microbial Fuel Cell Applications. *Int. J. Hydrog. Energy*  
35 495 **2024**, *57*, 679–687. <https://doi.org/10.1016/j.ijhydene.2024.01.043>.  
36 496 (11) Pandey, A.; Sahoo, S. Progress on Medical Implant: A Review and Prospects. *J. Bionic*  
37 497 *Eng.* **2023**, *20* (2), 470–494. <https://doi.org/10.1007/s42235-022-00284-z>.  
38 498 (12) Grech, J.; Antunes, E. Zirconia in Dental Prosthetics: A Literature Review. *J. Mater.*  
39 499 *Res. Technol.* **2019**, *8* (5), 4956–4964. <https://doi.org/10.1016/j.jmrt.2019.06.043>.  
40 500 (13) Romanos, G. E.; Fischer, G. A.; Delgado-Ruiz, R. Titanium Wear of Dental Implants  
41 501 from Placement, under Loading and Maintenance Protocols. *Int. J. Mol. Sci.* **2021**, *22* (3), 1067.  
42 502 <https://doi.org/10.3390/ijms22031067>.  
43 503 (14) Chappard, D.; Rony, L.; Ducellier, F.; Steiger, V.; Hubert, L. Wear Debris Released by  
44 504 Hip Prosthesis Analysed by Microcomputed Tomography. *J. Microsc.* **2021**, *282* (1), 13–20.  
45 505 <https://doi.org/10.1111/jmi.12971>.  
46 506 (15) Stricker, A.; Bergfeldt, T.; Fretwurst, T.; Addison, O.; Schmelzeisen, R.; Rothweiler,  
47 507 R.; Nelson, K.; Gross, C. Impurities in Commercial Titanium Dental Implants – A Mass and  
48 508 Optical Emission Spectrometry Elemental Analysis. *Dent. Mater.* **2022**, *38* (8), 1395–1403.  
49 509 <https://doi.org/10.1016/j.dental.2022.06.028>.  
50 510 (16) Gerken, L. R. H.; Gerdes, M. E.; Pruschy, M.; Herrmann, I. K. Prospects of  
51 511 Nanoparticle-Based Radioenhancement for Radiotherapy. *Mater. Horiz.* **2023**, *10* (10), 4059–  
52 512 4082. <https://doi.org/10.1039/D3MH00265A>.

- 1  
2  
3 513 (17) Sargazi, S.; Er, S.; Sacide Gelen, S.; Rahdar, A.; Bilal, M.; Arshad, R.; Ajalli, N.; Farhan  
4 514 Ali Khan, M.; Pandey, S. Application of Titanium Dioxide Nanoparticles in Photothermal and  
5 515 Photodynamic Therapy of Cancer: An Updated and Comprehensive Review. *J. Drug Deliv.*  
6 516 *Sci. Technol.* **2022**, *75*, 103605. <https://doi.org/10.1016/j.jddst.2022.103605>.  
7 517 (18) Gerken, L. R. H.; Beckers, C.; Brugger, B. A.; Kissling, V. M.; Gogos, A.; Wee, S.;  
8 518 Lukatskaya, M. R.; Schiefer, H.; Plasswilm, L.; Pruschy, M.; Herrmann, I. K. Catalytically  
9 519 Active Ti-Based Nanomaterials for Hydroxyl Radical Mediated Clinical X-Ray Enhancement.  
10 520 *Adv. Sci.* *n/a* (n/a), 2406198. <https://doi.org/10.1002/advs.202406198>.  
11 521 (19) Neufeld, M. J.; Lutzke, A.; Pratz, G.; Sun, C. High-Z Metal-Organic Frameworks for  
12 522 X-Ray Radiation-Based Cancer Theranostics. *Chem. Weinh. Bergstr. Ger.* **2021**, *27* (10), 3229–  
13 523 3237. <https://doi.org/10.1002/chem.202003523>.  
14 524 (20) Neuer, A. L.; Jessernig, A.; Gerken, L. R. H.; Gogos, A.; Starsich, F. H. L.; Anthis, A.  
15 525 H. C.; Herrmann, I. K. Cellular Fate and Performance of Group IV Metal Organic Framework  
16 526 Radioenhancers. *Biomater. Sci.* **2022**, *10* (22), 6558–6569.  
17 527 <https://doi.org/10.1039/D2BM00973K>.  
18 528 (21) Le Tourneau, C.; Hoffmann, C.; Takacs-Nagy, Z.; Liem, X.; Salas, S.; Debard, A.;  
19 529 Finzi, L.; Farber, L. A.; Gogishvili, M.; Kristesashvili, G.; Makharadze, T.; Yom, S. S.  
20 530 NANORAY-312: A Phase III Pivotal Study of NBTXR3 Activated by Investigator's Choice of  
21 531 Radiotherapy Alone or Radiotherapy in Combination with Cetuximab for Platinum-Based  
22 532 Chemotherapy-Ineligible Elderly Patients with Locally Advanced Head and Neck Squamous  
23 533 Cell Carcinoma. *J. Clin. Oncol.* **2022**, *40* (16\_suppl), TPS6110–TPS6110.  
24 534 [https://doi.org/10.1200/JCO.2022.40.16\\_suppl.TPS6110](https://doi.org/10.1200/JCO.2022.40.16_suppl.TPS6110).  
25 535 (22) Spiotto, M.; Feldman, L. E.; Luke, J. J.; Fleming, G. F.; Olson, D.; Moroney, J. W.;  
26 536 Nanda, R.; Rosenberg, A.; Pearson, A. T.; Juloori, A.; Weinberg, F.; Ray, C.; Gaba, R. C.;  
27 537 Chang, P. J.; Janisch, L. A.; Xu, Z.-Q.; Lin, W.; Weichselbaum, R. R.; Chmura, S. J. A Phase  
28 538 1 Dose-Escalation Study of RiMO-301 with Palliative Radiation in Advanced Tumors. *J. Clin.*  
29 539 *Oncol.* **2023**, *41* (16\_suppl), 2527. [https://doi.org/10.1200/JCO.2023.41.16\\_suppl.2527](https://doi.org/10.1200/JCO.2023.41.16_suppl.2527).  
30 540 (23) Bonvalot, S.; Rutkowski, P. L.; Thariat, J.; Carrère, S.; Ducassou, A.; Sunyach, M.-P.;  
31 541 Agoston, P.; Hong, A.; Mervoyer, A.; Rastrelli, M.; Moreno, V.; Li, R. K.; Tiangco, B.;  
32 542 Herraéz, A. C.; Gronchi, A.; Mangel, L.; Sy-Ortin, T.; Hohenberger, P.; de Baère, T.; Le Cesne,  
33 543 A.; Helfre, S.; Saada-Bouziid, E.; Borkowska, A.; Anghel, R.; Co, A.; Gebhart, M.; Kantor, G.;  
34 544 Montero, A.; Loong, H. H.; Vergés, R.; Lapeire, L.; Dema, S.; Kacso, G.; Austen, L.; Moureaux-  
35 545 Zabotto, L.; Servois, V.; Wardelmann, E.; Terrier, P.; Lazar, A. J.; Bovée, J. V. M. G.; Le  
36 546 Péchoux, C.; Papai, Z. NBTXR3, a First-in-Class Radioenhancer Hafnium Oxide Nanoparticle,  
37 547 plus Radiotherapy versus Radiotherapy Alone in Patients with Locally Advanced Soft-Tissue  
38 548 Sarcoma (Act.In.Sarc): A Multicentre, Phase 2–3, Randomised, Controlled Trial. *Lancet Oncol.*  
39 549 **2019**, *20* (8), 1148–1159. [https://doi.org/10.1016/S1470-2045\(19\)30326-2](https://doi.org/10.1016/S1470-2045(19)30326-2).  
40 550 (24) Grosse, S.; Haugland, H. K.; Lilleng, P.; Ellison, P.; Hallan, G.; Høl, P. J. Wear Particles  
41 551 and Ions from Cemented and Uncemented Titanium-Based Hip Prostheses—A Histological  
42 552 and Chemical Analysis of Retrieval Material. *J. Biomed. Mater. Res. B Appl. Biomater.* **2015**,  
43 553 *103* (3), 709–717. <https://doi.org/10.1002/jbm.b.33243>.  
44 554 (25) Shah, S.; Nene, S.; Rangaraj, N.; Raghuvanshi, R. S.; Singh, S. B.; Srivastava, S.  
45 555 Bridging the Gap: Academia, Industry and FDA Convergence for Nanomaterials. *Drug Dev.*  
46 556 *Ind. Pharm.* **2020**, *46* (11), 1735–1746. <https://doi.org/10.1080/03639045.2020.1821055>.  
47 557 (26) Li, Y.; Qi, Y.; Zhang, H.; Xia, Z.; Xie, T.; Li, W.; Zhong, D.; Zhu, H.; Zhou, M. Gram-  
48 558 Scale Synthesis of Highly Biocompatible and Intravenous Injectable Hafnium Oxide  
49 559 Nanocrystal with Enhanced Radiotherapy Efficacy for Cancer Theranostic. *Biomaterials* **2020**,  
50 560 *226*, 119538. <https://doi.org/10.1016/j.biomaterials.2019.119538>.

- 1  
2  
3 561 (27) Yu, N.; Tu, W.; Qiu, P.; Ren, Q.; Chen, X.; Zhu, M.; Liu, Y.; Chen, Z. Full-Route  
4 562 Advances via Biomimetic and Biodegradable Ultrasmall-in-Nano Architectures with  
5 563 Radiation-Photo Synergy. *Nano Today* **2022**, *43*, 101427.  
6 564 <https://doi.org/10.1016/j.nantod.2022.101427>.  
7 565 (28) L. McGinnity, T.; Dominguez, O.; E. Curtis, T.; D. Nallathamby, P.; J. Hoffman, A.;  
8 566 K. Roeder, R. Hafnia (HfO<sub>2</sub>) Nanoparticles as an X-Ray Contrast Agent and Mid-Infrared  
9 567 Biosensor. *Nanoscale* **2016**, *8* (28), 13627–13637. <https://doi.org/10.1039/C6NR03217F>.  
10 568 (29) Holleman, A. F. *Lehrbuch Der Anorganischen Chemie*, 102nd ed.; Walter de Gruyter  
11 569 GmbH & Co KG, 2007; p. 1535.  
12 570 (30) Mutsuga, M.; Sato, K.; Hirahara, Y.; Kawamura, Y. Analytical Methods for SiO<sub>2</sub> and  
13 571 Other Inorganic Oxides in Titanium Dioxide or Certain Silicates for Food Additive  
14 572 Specifications. *Food Addit. Contam. Part A* **2011**, *28* (4), 423–427.  
15 573 <https://doi.org/10.1080/19440049.2010.551548>.  
16 574 (31) Salvador, A.; Pascual-Martí, M. C.; Adell, J. R.; Requeni, A.; March, J. G. Analytical  
17 575 Methodologies for Atomic Spectrometric Determination of Metallic Oxides in UV Sunscreen  
18 576 Creams. *J. Pharm. Biomed. Anal.* **2000**, *22* (2), 301–306. [https://doi.org/10.1016/S0731-7085\(99\)00286-1](https://doi.org/10.1016/S0731-7085(99)00286-1).  
19 577 (32) Khosravi, K.; Hoque, M. E.; Dimock, B.; Hintelmann, H.; Metcalfe, C. D. A Novel  
20 578 Approach for Determining Total Titanium from Titanium Dioxide Nanoparticles Suspended in  
21 579 Water and Biosolids by Digestion with Ammonium Persulfate. *Anal. Chim. Acta* **2012**, *713*,  
22 580 86–91. <https://doi.org/10.1016/j.aca.2011.11.048>.  
23 581 (33) Kim, N.; Kim, C.; Jung, S.; Park, Y.; Lee, Y.; Jo, J.; Hong, M.; Lee, S.; Oh, Y.; Jung,  
24 582 K. Determination and Identification of Titanium Dioxide Nanoparticles in Confectionery  
25 583 Foods, Marketed in South Korea, Using Inductively Coupled Plasma Optical Emission  
26 584 Spectrometry and Transmission Electron Microscopy. *Food Addit. Contam. Part A* **2018**, *35*  
27 585 (7), 1238–1246. <https://doi.org/10.1080/19440049.2018.1482011>.  
28 586 (34) Holleman, A. F. *Lehrbuch Der Anorganischen Chemie*, 102nd ed.; Walter de Gruyter  
29 587 GmbH & Co KG, 2007; p.1539.  
30 588 (35) Ma, Y.; Stopic, S.; Gronen, L.; Friedrich, B. Recovery of Zr, Hf, Nb from Eudialyte  
31 589 Residue by Sulfuric Acid Dry Digestion and Water Leaching with H<sub>2</sub>O<sub>2</sub> as a Promoter.  
32 590 *Hydrometallurgy* **2018**, *181*, 206–214. <https://doi.org/10.1016/j.hydromet.2018.10.002>.  
33 591 (36) Watkins, P. S.; Castellon, B. T.; Tseng, C.; Wright, M. V.; Matson, C. W.; Cobb, G. P.  
34 592 Validation of a Sulfuric Acid Digestion Method for Inductively Coupled Plasma Mass  
35 593 Spectrometry Quantification of TiO<sub>2</sub> Nanoparticles. *Bull. Environ. Contam. Toxicol.* **2018**, *100*  
36 594 (6), 809–814. <https://doi.org/10.1007/s00128-018-2336-2>.  
37 595 (37) Neuer, A. L.; Geck, D.; Gogos, A.; Kissling, V. M.; Balfourier, A.; Herrmann, I. K.  
38 596 Nanoanalytical Insights into the Stability, Intracellular Fate, and Biotransformation of Metal–  
39 597 Organic Frameworks. *ACS Appl. Mater. Interfaces* **2023**, *15* (32), 38367–38380.  
40 598 <https://doi.org/10.1021/acsami.3c08818>.  
41 599 (38) Schmidt, H. G. Safe Piranhas: A Review of Methods and Protocols. *ACS Chem. Health*  
42 600 *Saf.* **2022**, *29* (1), 54–61. <https://doi.org/10.1021/acs.chas.1c00094>.  
43 601 (39) Rudek, B.; McNamara, A.; Ramos-Méndez, J.; Byrne, H.; Kuncic, Z.; Schuemann, J.  
44 602 Radio-Enhancement by Gold Nanoparticles and Their Impact on Water Radiolysis for x-Ray,  
45 603 Proton and Carbon-Ion Beams. *Phys. Med. Biol.* **2019**, *64* (17), 175005.  
46 604 <https://doi.org/10.1088/1361-6560/ab314c>.  
47 605 (40) Liem, X.; de Baère, T.; Vivar, O. I.; Seiwert, T. Y.; Shen, C.; Pápai, Z.; Moreno, V.;  
48 606 Takácsi-Nagy, Z.; Helfferich, F.; Thariat, J.; Gooi, Z.; Yom, S. S.; Bossi, P.; Ferris, R. L.;  
49 607 Hackman, T. G.; Le Tourneau, C.; Rodriguez, J.; Hoffmann, C. International Guidelines for  
50 608

- 609 Intratumoral and Intranodal Injection of NBTXR3 Nanoparticles in Head and Neck Cancers. *View Article Online*  
610 *Head Neck* **2024**, *46* (6), 1253–1262. <https://doi.org/10.1002/hed.27739>. DOI: 10.1039/D5AY00731C
- 611 (41) Kromidas, S. *Validierung in der Analytik*; Die Praxis der instrumentellen Analytik;  
612 Wiley-VCH: Weinheim, 2012.
- 613 (42) Doebelin, N.; Kleeberg, R. Profex: A Graphical User Interface for the Rietveld  
614 Refinement Program BGMN. *J. Appl. Crystallogr.* **2015**, *48* (5), 1573–1580.  
615 <https://doi.org/10.1107/S1600576715014685>.
- 616 (43) FDA. *Q2(R2) Validation of Analytical Procedures*. [https://www.fda.gov/regulatory-](https://www.fda.gov/regulatory-information/search-fda-guidance-documents/q2r2-validation-analytical-procedures)  
617 [information/search-fda-guidance-documents/q2r2-validation-analytical-procedures](https://www.fda.gov/regulatory-information/search-fda-guidance-documents/q2r2-validation-analytical-procedures) (accessed  
618 2025-04-24).
- 619 (44) He, H.; Xu, F.; Li, Q.; Dong, P.; Zheng, J.; Wu, C.; He, Z.; Qu, J.; Xu, Z.; Chi, R.; Wu,  
620 M. Separation of Hafnium from Zirconium in HNO<sub>3</sub> Solution by Solvent Extraction with  
621 Cyanex572. *Hydrometallurgy* **2021**, *202*, 105600.  
622 <https://doi.org/10.1016/j.hydromet.2021.105600>.
- 623 (45) Wang, L. Y.; Lee, M. S. A Review on the Aqueous Chemistry of Zr(IV) and Hf(IV) and  
624 Their Separation by Solvent Extraction. *J. Ind. Eng. Chem.* **2016**, *39*, 1–9.  
625 <https://doi.org/10.1016/j.jiec.2016.06.004>.
- 626 (46) HfO<sub>2</sub> Monoclinic - MP ID: Mp-352. [https://next-](https://next-gen.materialsproject.org/materials/mp-352)  
627 [gen.materialsproject.org/materials/mp-352](https://next-gen.materialsproject.org/materials/mp-352).
- 628 (47) ZrO<sub>2</sub> Monoclinic - MP ID: Mp-2858. [https://next-](https://next-gen.materialsproject.org/materials/mp-2858)  
629 [gen.materialsproject.org/materials/mp-2858](https://next-gen.materialsproject.org/materials/mp-2858).
- 630 (48) TiO<sub>2</sub> Anatase - MP ID: Mp-390. [https://next-gen.materialsproject.org/materials/mp-](https://next-gen.materialsproject.org/materials/mp-390)  
631 [390](https://next-gen.materialsproject.org/materials/mp-390).
- 632 (49) TiO<sub>2</sub> Rutile - MP ID: Mp-2657. [https://next-gen.materialsproject.org/materials/mp-](https://next-gen.materialsproject.org/materials/mp-2657)  
633 [2657](https://next-gen.materialsproject.org/materials/mp-2657).
- 634 (50) HfO<sub>2</sub> Orthorhombic - MP ID: Mp-1858. [https://next-](https://next-gen.materialsproject.org/materials/mp-1858)  
635 [gen.materialsproject.org/materials/mp-1858](https://next-gen.materialsproject.org/materials/mp-1858).
- 636 (51) Wang, Z.; Ni, Z.; Qiu, D.; Tao, G.; Yang, P. Determination of Impurities in Titanium  
637 Nitride by Slurry Introduction Axial Viewed Inductively Coupled Plasma Optical Emission  
638 Spectrometry. *Spectrochim. Acta Part B At. Spectrosc.* **2005**, *60* (3), 361–367.  
639 <https://doi.org/10.1016/j.sab.2004.12.006>.
- 640 (52) Ebdon, L.; Foulkes, M.; Sutton, K. Slurry Nebulization in Plasmas. *J. Anal. At.*  
641 *Spectrom.* **1997**, *12* (2), 213–229. <https://doi.org/10.1039/A604914A>.
- 642 (53) Moltved, K. A.; Kepp, K. P. The Chemical Bond between Transition Metals and  
643 Oxygen: Electronegativity, d-Orbital Effects, and Oxophilicity as Descriptors of Metal–  
644 Oxygen Interactions. *J. Phys. Chem. C* **2019**, *123* (30), 18432–18444.  
645 <https://doi.org/10.1021/acs.jpcc.9b04317>.
- 646



Empa

Materials Science and Technology  
View Article Online  
DOI: 10.1039/D5AY00731C

**Data availability**

The data supporting this article have been included as part of the Supplementary Information.

Analytical Methods Accepted Manuscript

1  
2  
3  
4  
5  
6  
7  
8  
9  
10  
11  
12  
13  
14  
15  
16  
17  
18  
19  
20  
21  
22  
23  
24  
25  
26  
27  
28  
29  
30  
31  
32  
33  
34  
35  
36  
37  
38  
39  
40  
41  
42  
43  
44  
45  
46  
47  
48  
49  
50  
51  
52  
53  
54  
55  
56  
57  
58  
59  
60

Downloaded on 03 June 2025 at 06:33:28 AM.  
This article is licensed under a Creative Commons Attribution 3.0 Unported Licence.